Inorg. Chem. **2008**, *47*, 8324−8335

Modulation of Metal Displacements in a Saddle Distorted Macrocycle: Synthesis, Structure, and Properties of High-Spin Fe(III) Porphyrins and Implications for the Hemoproteins

Ranjan Patra, Arvind Chaudhary, Sudip Kumar Ghosh, and Sankar Prasad Rath*

Department of Chemistry, Indian Institute of Technology Kanpur, Kanpur-208016, India

Received May 25, 2008

A rare family of five and six-coordinated high-spin Fe(III) porphyrins incorporating weak axial ligands are synthesized and structurally characterized which demonstrate, for the first time, stepwise metal displacements in a single distorted macrocyclic environment that has generally been seen in many biological systems. The introduction of four nitro groups into the *meso*-positions of octaethyl porphyrin severely distorts the porphyrin geometry and provides an interesting modulation of the macrocycle properties which enables the facile isolation of "pure" high-spin Fe^{III}(*tn*-OEP)Cl, Fe^{III}(*tn*-OEP)(MeOH)Cl, and Fe^{III}(*tn*-OEP)$(H_2O)_2^+$ in excellent yields in a saddle distorted macrocyclic environment that are known to stabilize intermediate spin states. The stepwise out-of-plane displacements of iron are as follows: 0.47 Å for Fe^{III}(*tn*-OEP)Cl; 0.09 Å for Fe^{III}(*tn*-OEP)(MeOH)Cl, and 0.01 Å for Fe^{III}(*tn*-OEP)$(H_2O)_2^+$ from the mean plane of the porphyrins. However, in both five and six-coordinated Fe(III) porphyrins, the Fe−Np distances are quite comparable while the porphyrin cores have expanded significantly, virtually to the same extent for the six-coordinate complexes reported here. The large size of the high-spin iron(III) atom in Fe^{III}(*tn*-OEP)$(H_2O)_2^+$ is accommodated perfectly with no displacement of the metal. This expansion is accompanied by a significant decrease of the saddle distortion with a clear increase of the ruffling. Furthermore, the Fe atom in Fe^{III}(*tn*-OEP)(MeOH)Cl is not out of plane because of the larger atom size; however, the displacement of the iron depends on both the relative strength of the axial ligands, as well as the nature and extent of the ring deformation. Our characterization demonstrates that increase in ruffling and/or decrease in macrocycle deformation brings the iron atom more into the plane in a distorted macrocyclic environment. Our observations thus suggest that the displacements of iron in proteins are the consequences of nonequivalent axial coordination, as well as protein induced deformations at the heme. The high-spin nature of the complexes reported here is believed to be due to the larger Fe−Np distances which then reduce substantially the interaction between iron $d_{x^2-y^2}$ and porphyrin a_{2u} orbital. The Fe^{III}/Fe^{II} reduction potential of Fe^{III}(*tn*-OEP)Cl shows a reversible peak at large positive value (0.20 V), and no ring-centered oxidation was observed within the solvent limit (∼1.80 V). It is thus easier to reduce Fe^{III}(*tn*-OEP)Cl by almost 700 mV compared to Fe^{III}(OEP)Cl while oxidations are very difficult. Furthermore, the addition of 3-Cl-pyridine to Fe^{III}(*tn*-OEP)Cl in air undergoes spontaneous auto reduction to produce the rare air-stable Fe^{II}(*tn*-OEP)(3-Cl-py)$_2$ that shows Fe^{II}/Fe^{III} oxidation peaks at high positive potential (0.79 V), which is ∼600 mV more anodic compared to $[Fe^{II}$(*tn*-OEP)Cl$]^-$. This large anodic shift illustrates the effective removal of metal-centered electron density by the macrocycle when the metal is constrained to reside in the porphyrin plane.

Introduction

The structural and electronic effects of peripheral substitution of the porphyrin macrocycle have been the subject of numerous theoretical and experimental investigations for a long time.[1−8] Nonplanar distortions of the porphyrin macrocycle, which result from steric interactions among the peripheral substitutions, have been investigated to understand the functional consequences of similar distortions observed

* To whom correspondence should be addressed. E-mail: sprath@iitk.ac.in.

(1) (a) Senge, M. O. In *The Porphyrin Handbook*; Kadish, K. M., Smith, K. M., Guilard, R., Eds.; Academic Press: San Diego, 2000; Vol. *1*, p 239. (b) Senge, M. O. *Chem. Commun.* **2006**, 243.

10.1021/ic800944q CCC: $40.75
Published on Web 08/14/2008

in various proteins.[1−5] The conformational variations offer an attractive mechanism for the modulation of a wide range of physical and chemical properties of porphyrins in vitro and in vivo which has led to the synthesis of and structural studies on a large number of sterically crowded porphyrins.[1−8] Saddle-shaped iron(III) porphyrins have been shown to be very promising models for the heme centers in the cytochrome bc_1 complex and other heme proteins.[4,5]

A typical five-coordinate ferric porphyrin has a small amount of doming, and the metal ion is displaced by ∼0.45 Å toward the axial ligand from the mean porphyrin plane.[1−5] On the other hand, the six-coordinate high-spin ferric heme has an essentially flat porphyrin core with no doming where the metal atom sits in the plane of the porphyrins. However, the crystal structure of horse methemoglobin reveals small displacement of the iron atom from the heme plane (0.07 Å in the α chains and 0.21 Å in the β chains).[9] Whether the displacements of the iron atom in proteins like aquomethemoglobin are a consequence of the nonequivalent axial coordination or a feature of protein controlled stereochemistry at the heme is an interesting question.[10] Herein we wish to report a rare family of five and six-coordinated high-spin Fe(III) porphyrins where the structural diversity are modulated stepwise (Chart 1), for the first time, in a single distorted macrocycle environment. This enabled us to scrutinize the effects of axial ligand coordination and macrocycle nonplanarity on metal ion displacement that has generally been recognized in many biological systems. The different conformational landscapes observed further illustrate the plasticity of the macrocycles, as well as their acute structural sensitivity to their microenvironment. We also would like to investigate whether the nature and extent of macrocyclic deformations are associated with unusual Fe(III/II) electronic structures and properties to understand the effects of similar distortions in biology.

Chart 1

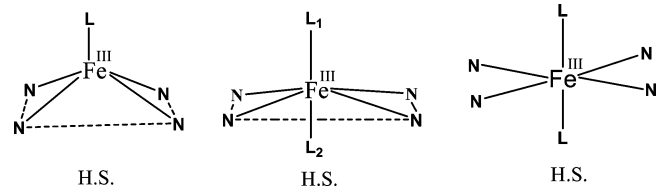

Results and Discussion

Porphyrin macrocycles can be distorted via the introduction of sterically demanding substituents in the porphyrin periphery. For this, we have synthesized tetra nitrooctaethyl porphyrin (*tn*-H_2OEP) which because of its highly saddle-distorted geometry and also the presence of four electron-withdrawing *meso*-nitro groups provides an interesting modulation of the macrocycle properties. The free ligand (*tn*-H_2OEP) has been synthesized via demetalation of Zn tetranitro octaethyl porphyrin as reported previously,[11] and the iron metal is inserted by refluxing the ligand in dimethylformamide (DMF) with $FeCl_2$ under nitrogen for nearly 2.5 h followed by chromatographic separation in silica gel using chloroform as eluent to form Fe^{III}(*tn*-OEP)Cl in excellent yields. The UV−vis spectrum of the molecule shows Soret and Q-bands at 378, 425, and 668 nm, which is similar to those of other high-spin five coordinated Fe(III) porphyrins. However, addition of weak MeOH ligands into the benzene solution of Fe^{III}(*tn*-OEP)Cl slightly red-shifted the Soret and Q bands to 381, 431, and 670 nm, which was then isolated in excellent yields and characterized as Fe^{III}(*tn*-OEP)(MeOH)Cl. We have also synthesized and characterized Fe^{III}(*tn*-OEP)$(H_2O)_2$·ClO_4 in good yields and details are given in the Experimental Section. Although five-coordinated Fe^{III}(*tn*-OEP)Cl is common, Fe^{III}(*tn*-OEP)(MeOH)Cl and

(2) (a) Shelnutt, J. A. In *The Porphyrin Handbook*; Kadish, K. M., Smith, K. M., Guilard, R., Eds.; Academic Press: New York, 2000; 167; Vol. *7*. (b) Shelnutt, J. A.; Song, X.-Z.; Ma, J.-G.; Jia, S.-L.; Jentzen, W.; Medforth, C. J. *Chem. Soc. Rev.* **1998**, *27*, 31. (c) Ravikanth, M.; Chandrashekar, T. K. *Structure and Bonding*; Springer: Berlin, 1995; Vol. *82*, p 107.

(3) (a) Scheidt, W. R. In *The Porphyrin Handbook*; Kadish, K. M., Smith, K. M., Guilard, R., Eds.; Academic Press: San Diego, 2000; Vol. *3*, pp. 49. (b) Scheidt, W. R.; Reed, C. A. *Chem. Rev.* **1981**, *81*, 543.

(4) (a) Walker, F. A. *Chem. Rev.* **2004**, *104*, 589. (b) Yatsunyk, L. A.; Shokhirev, N. V.; Walker, F. A. *Inorg. Chem.* **2005**, *44*, 2848. (c) Yatsunyk, L. A.; Walker, F. A. *Inorg. Chem.* **2004**, *43*, 4341. (d) Walker, F. A. *Coord. Chem. Rev.* **1999**, *186*, 471.

(5) (a) Nakamura, M.; Ohgo, Y.; Ikezaki, A. *J. Inorg. Biochem.* **2008**, *102*, 433. (b) Nakamura, M. *Coord. Chem. Rev.* **2006**, *250*, 2271. (c) Ohgo, Y.; Chiba, Y.; Hashizume, D.; Uekusa, H.; Ozekie, T.; Nakamura, M. *Chem. Commun.* **2006**, 1935. (d) Ikeue, T.; Ohgo, Y.; Ongayi, O.; Vicente, M. G. H.; Nakamura, M. *Inorg. Chem.* **2003**, *42*, 5560. (e) Nakamura, M.; Takahisa Ikeue, T.; Ohgo, Y.; Takahashi, M.; Takeda, M. *Chem. Commun.* **2002**, 1198. (f) Ikeue, T.; Ohgo, Y.; Yamaguchi, T.; Takahashi, M.; Takeda, M.; Nakamura, M. *Angew. Chem., Int. Ed.* **2001**, *40*, 2617. (g) Ikeue, T.; Saitoh, T.; Yamaguchi, T.; Ohgo, Y.; Nakamura, M.; Takahashi, M.; Takeda, M. *Chem. Commun.* **2000**, 1989. (h) Ohgo, Y.; Ikeue, T.; Nakamura, M. *Inorg. Chem.* **2002**, *41*, 1698.

(6) (a) Cheng, R.-J.; Wang, Y.-K.; Chen, P.-Y.; Han, Y.-P.; Chang, C.-C. *Chem. Commun.* **2005**, 1312. (b) Cheng, R.-J.; Chen, P.-Y.; Lovell, T.; Liu, T.; Noodleman, L.; Case, D. A. *J. Am. Chem. Soc.* **2003**, *125*, 6774. (c) Cheng, R.-J.; Chen, P.-Y.; Gau, P.-R.; Chen, C.-C.; Peng, S.-M. *J. Am. Chem. Soc.* **1997**, *119*, 2563.

(7) (a) Schünemann, V.; Gerdan, M.; Trautwein, A. X.; Haoudi, N.; Mandon, D.; Fischer, J.; Weiss, R.; Tabard, A.; Guilard, R. *Angew. Chem., Int. Ed.* **1999**, *38*, 3181. (b) Guillemot, M.; Toupet, L.; Simonneaux, G. *Inorg. Chem.* **1996**, *35*, 6334. (c) Renner, M. W.; Barkigia, K. M.; Zhang, Y.; Medforth, C. J.; Smith, K. M.; Fajer, J. *J. Am. Chem. Soc.* **1994**, *116*, 8582. (d) Barkigia, K. M.; Dolores Berber, M.; Fajer, J.; Medforth, C. J.; Renner, M. W.; Smith, K. M. *J. Am. Chem. Soc.* **1990**, *112*, 8851.

(8) (a) Ohgo, Y.; Hoshino, A.; Okamura, T.; Uekusa, H.; Hashizume, D.; Ikezaki, A.; Nakamura, M. *Inorg. Chem.* **2007**, *46*, 8193. (b) Shao, J.; Steene, E.; Hoffman, B. M.; Ghosh, A. *Eur. J. Inorg. Chem.* **2005**, 1609. (c) Hoshino, A.; Ohgo, Y.; Nakamura, M. *Inorg. Chem.* **2005**, *44*, 7333. (d) Zakharieva, O.; Schunemann, V.; Gerdan, M.; Licoccia, S.; Cai, S.; Walker, F. A.; Trautwein, A. X. *J. Am. Chem. Soc.* **2002**, *124*, 6636. (e) Steene, E.; Wondimagegn, T.; Ghosh, A. *J. Phys. Chem. B* **2001**, *105*, 11406. (f) Ghosh, A.; Harvorsen, I.; Nilsen, H. J.; Steene, E.; Wondimagegn, T.; Lie, R.; van Caemelbecke, E.; Guuo, N.; Ou, Z.; Kadish, K. M. *J. Phys. Chem. B* **2001**, *105*, 8120. (g) Ghosh, A.; Vangberg, T.; Gonzalez, E.; Taylor, P. J. *J. Porphyrins Phthalocyanines* **2001**, *5*, 345. (h) Simonneaux, G.; Schunemann, V.; Morice, C.; Carel, L.; Toupet, L.; Winkler, H.; Trautwein, A. X.; Walker, F. A. *J. Am. Chem. Soc.* **2000**, *122*, 4366. (i) Cheng, R.-J.; Chen, P.-Y. *Chem.—Eur. J.* **1999**, *5*, 1708.

(9) (a) Ladner, R. C.; Heidner, E. J.; Perutz, M. F. *J. Mol. Biol.* **1977**, *114*, 385. (b) Takano, T. *J. Mol. Biol.* **1977**, *110*, 537.

(10) (a) Scheidt, W. R.; Lee, Y. J.; Tamai, S.; Hatano, K. *J. Am. Chem. Soc.* **1983**, *105*, 778. (b) Spiro, T. G.; Stong, J. D.; Stein, P. *J. Am. Chem. Soc.* **1978**, *101*, 2648. (c) Mashiko, T.; Kastner, M. E.; Spontalian, K.; Scheidt, W. R.; Reed, C. A. *J. Am. Chem. Soc.* **1978**, *100*, 6354. (d) Messana, C.; Massimo, C.; Shenkin, P.; Noble, R. W.; Fermi, G.; Perutz, R. N.; Perutz, M. F. *Biochemistry* **1978**, *17*, 3652.

(11) Gong, L.; Dolphin, D. *Can. J. Chem.* **1985**, *63*, 401.

Scheme 1

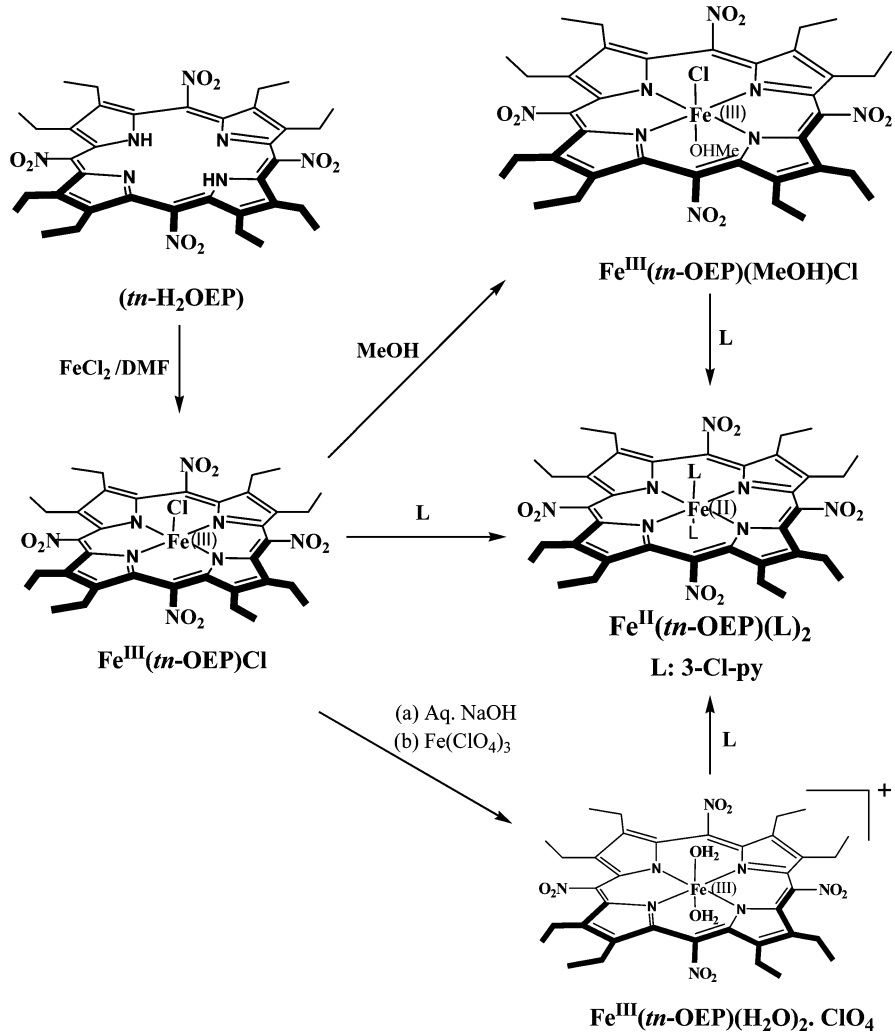

Fe^{III}(*tn*-OEP)$(H_2O)_2^+$ authenticate very rare examples of six-coordinate high-spin Fe(III) complexes in a saddle distorted macrocyclic environment as shown in Scheme 1 and provide a reference point for the discussion of protein-controlled nuances of the high-spin state. In contrast, saddle shaped porphyrins are known to stabilize the intermediate spin states of Fe(III) with weak axial ligands.[5−8]

However, addition of 3-Cl-pyridine to Fe^{III}(*tn*-OEP)Cl in air undergoes spontaneous auto reduction to produce the rare air-stable six-coordinate Fe^{II}(*tn*-OEP)(3-Cl-py)$_2$ in solution (Scheme 1); Figure 1 shows the gradual changes in UV−visible spectra of Fe^{III}(*tn*-OEP)Cl in the presence of varying amounts of 3-Cl-pyridine in which the peaks at 426, 548, and 584 nm corresponding to six-coordinate Fe^{II}(*tn*-OEP)(3-Cl-py)$_2$ are gaining in intensity while the peaks corresponding to Fe^{III}(*tn*-OEP)Cl decrease in intensity. Similar observations are also obtained when other axial ligands such as pyridine and imidazoles are used as axial ligands.[12]

Crystallographic Characterization of Fe^{III}(*tn*-OEP)Cl. The molecule crystallizes via slow evaporation of the chloroform solutions of the compound in the monoclinic crystal system with a *C*2/*c* space group. A perspective view is shown in Figure 2, and the selected bond distances and angles are given in Table 1 while crystal data and data collection parameters are given in Table 2. The complex has a five coordinate square-pyramidal geometry in which the iron atom is displaced by 0.46 Å from the N4 plane, a distance which is in the range of 0.39−0.54 Å seen for other high-spin, five-coordinate iron(III) porphyrins.[3−5] The average Fe−Np and Fe−Cl distances are found to be 2.067(3) Å and 2.1918(10) Å, respectively. Thus, the observed Fe−Np (average) distance is significantly long while the Fe−Cl distance is relatively short compared to similar complexes with a distorted macrocycle.[5−7] For example, the mean Fe−Np bond lengths are 2.040(6) and 2.031(5) Å, and the Fe−Cl bond lengths are 2.233(1) and 2.242(2) Å in the two crystalline forms of Fe^{III}(OETPP)Cl.[6c,7a]

Crystallographic Characterization of Fe^{III}(*tn*-OEP)(MeOH)Cl. Dark brown crystals were grown by slow diffusion of CH_3OH into a benzene solution of Fe^{III}(*tn*-OEP)Cl at room temperature. Methanol is a ligand that is certainly not noted for its strong complexing power. However, the presence of four electron-withdrawing bulky nitro groups at the *meso* positions provides an interesting modulation of the macrocycle properties which enables the facile formation and isolation of high-spin iron(III) porphyrin with

(12) Patra, R.; Rath, S. P. unpublished results.

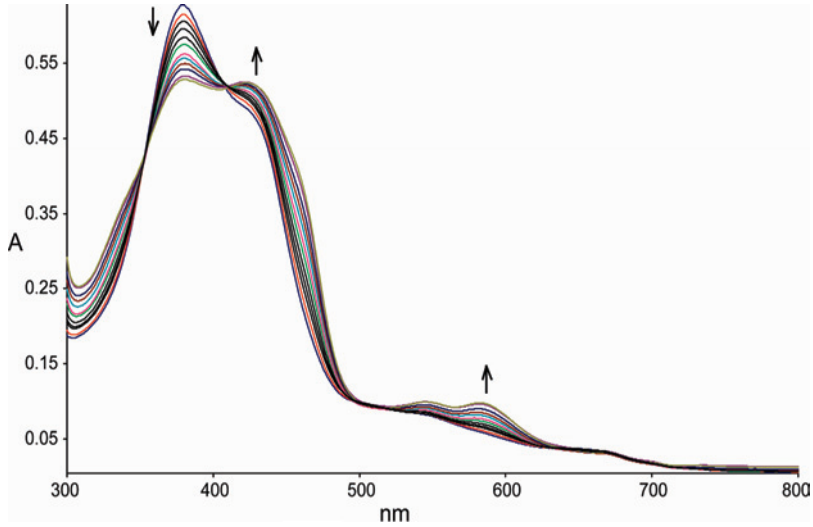

Figure 1. Spectral change of Fe^{III}(*tn*-OEP)Cl in chloroform in the presence of varying amount of 3-Cl-pyridine forming six-coordinated Fe^{II}(*tn*-OEP)(3-Cl-py)$_2$, arrows indicate increase or decrease of band intensity. Isosbestic points (nm): 360, 402, and 496.

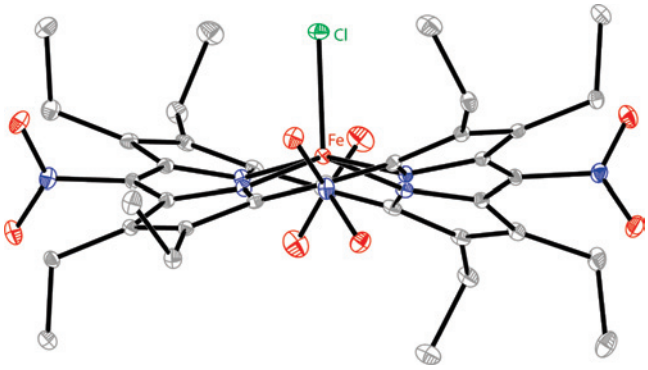

Figure 2. Perspective view of Fe^{III}(*tn*-OEP)Cl showing 50% thermal contours for all non-hydrogen atoms at 100 K (H-atoms have been omitted for clarity).

inequivalent axial ligands, for the first time, in a distorted macrocyclic environment. The molecule crystallizes in the monoclinic crystal system with *P*2(1)/*n* space group, and a perspective view is shown in Figure 3. The selected bond distance and angles are given in Table 1, and crystal data and data collection parameters are shown in Table 2.

Figure 4 shows the H-bonding interactions between the methanolic hydrogen of one molecule and the axial chloride ligand of the other molecule forming an infinite chain in the molecular packing. The Fe−Np distances, which range from 2.062(3) to 2.066(3) Å, leave little doubt that the Fe(III) ion is high-spin since these distances are much longer than the range of 1.97−2.00 Å found for six-coordinated low-spin ferric porphyrins.[3−5] Furthermore, the average Fe−Np bond distance of 2.064(3) Å is also larger than the average values of 2.048(4) Å and 2.05(3) Å observed for the only other two structurally characterized,[13] unsymmetrically substituted, high-spin ferric porphyrins. There is, however, a ∼0.11 Å lengthening of the Fe−Cl bond that occurs in Fe^{III}(*tn*-OEP)(MeOH)Cl compared to the "normal" Fe−Cl length

Table 1. Selected Bond Distances (Å) and Angles (deg)

	Fe^{III}(*tn*-OEP)Cl	Fe^{III}(*tn*-OEP)(MeOH)Cl	Fe^{III}(*tn*-OEP)$(H_2O)_2\cdot ClO_4$
	Bond Lengths, (Å)		
Fe1−N1	2.066(3)	2.065(3)	2.061(2)
Fe1−N2	2.063(3)	2.062(3)	2.059(2)
Fe1−N3	2.060(3)	2.063(3)	2.068(2)
Fe1−N4	2.078(3)	2.066(3)	2.055(2)
Fe1−Cl	2.1918(10)	2.3049(11)	
Fe1−O9		2.170(3)	2.0697(18)
Fe1−O10			2.0695(18)
	Bond Angles, (deg)		
N(1)−Fe−N(2)	87.51(11)	89.79(12)	89.55(9)
N(1)−Fe−N(3)	160.13(11)	169.62(13)	177.55(8)
N(1)−Fe−N(4)	86.36(10)	90.02(12)	90.33(9)
N(2)−Fe−N(3)	87.68(11)	89.45(12)	90.69(9)
N(2)−Fe−N(4)	147.84(11)	175.55(13)	177.19(8)
N(3)−Fe−N(4)	87.50(11)	89.94(12)	89.55(9)
N(1)−Fe−Cl(1)	100.94(8)	94.86(9)	
N(2)−Fe−Cl(1)	104.86(8)	91.95(10)	
N(3)−Fe−Cl(1)	98.93(8)	95.52(9)	
N(4)−Fe−Cl(1)	107.30(8)	92.50(9)	
N(1)−Fe−O(9)		86.48(11)	90.04(8)
N(2)−Fe−O(9)		87.31(12)	89.05(8)
N(3)−Fe−O(9)		83.14(11)	87.52(8)
N(4)−Fe−O(9)		88.24(12)	93.76(8)
N(1)−Fe−O(10)			89.87(8)
N(2)−Fe−O(10)			90.72(8)
N(3)−Fe−O(10)			92.57(8)
N(4)−Fe−O(10)			86.47(8)

observed in the five-coordinate high-spin complex Fe^{III}(*tn*-OEP)Cl (Table 1). The axial Fe−O distance of 2.170(3) Å is also slightly larger than the reported 2.136(8) Å for the similar distance in high-spin $Fe^{III}(OEP)(EtOH)_2\cdot ClO_4$.[14a] However, the iron atom is displaced 0.09 Å out of the mean porphyrin plane (24 atom) and 0.13 Å out of the mean plane of the four porphinato nitrogens in the direction of the axial chloride ligand. Although the MeOH is a relatively strong field ligand, this is outweighed for the high-spin Fe^{3+} ion by the negative charge on the Cl^-. Axial bond distances are thus consistent with a substantially stronger bond to the chloride ligand. It is of interest in this connection that in Mn^{III}(TPP)(py)Cl,[14b] the Mn atom is also displaced toward the chloride ion by 0.145 Å from the mean

(13) (a) Kellett, P. J.; Pawlik, M. J.; Taylor, L. F.; Thompson, R. G.; Levstik, M. A.; Anderson, O. P.; Strauss, S. H. *Inorg. Chem.* **1989**, *28*, 440. (b) Scheidt, W. R.; Lee, Y. J.; Geiger, D. K.; Taylor, K.; Hatano, K. *J. Am. Chem. Soc.* **1982**, *104*, 3367.

Table 2. Crystal Data and Data Collection Parameters

	Fe^{III}(*tn*-OEP)Cl	Fe^{III}(*tn*-OEP)(MeOH)Cl	Fe^{III}(*tn*-OEP)$(H_2O)_2$ ClO_4 2THF
T, K	100(2)	100(2)	100(2)
formula	C_{36} H_{40} Cl Fe N_8 O_8	C_{37} H_{44} Cl Fe N_8 O_9	C_{44} H_{60} Cl Fe N_8 O_{16}
formula weight	804.06	836.10	1048.30
color and habit	dark brown	dark brown	dark brown
crystal system	monoclinic	monoclinic	triclinic
space group	*C*2/*c*	*P*2(1)/*n*	$P\bar{1}$
a, Å	33.627(3)	6.5854(5)	9.7589(15)
b, Å	13.8423(11)	44.780(3)	10.3685(16)
c, Å	19.8719(16)	13.2963(10)	24.456(4)
α, deg	90	90	94.909(2)
β, deg	126.1390(10)	96.954(2)	97.976(2)
γ, deg	90	90	98.321(2)
V, $Å^3$	7470.1(10)	3892.1(5)	2410.7(6)
radiation (*λ*, Å)	Mo Kα (0.71073)	Mo Kα (0.71073)	Mo Kα (0.71073)
Z	8	4	2
d_{calcd}, $g \cdot cm^{-3}$	1.430	1.427	1.444
μ, mm^{-1}	0.538	0.521	0.447
F(000)	3352	1748	1102
no. of unique data	7720	8455	8283
no. of restraints	0	0	6
no. of params. refined	495	524	648
GOF on F^2	1.012	1.020	1.035
$R1^a$ [$I > 2\sigma(I)$]	0.0548	0.0659	0.0514
$R1^a$ (all data)	0.0932	0.1178	0.0654
$wR2^b$ (all data)	0.1444	0.1680	0.1470

^{a} $R1 = \sum||F_o| - |F_c||/\sum|F_o|$. ^{b} $wR2 = \{\sum[w(F_o^2-F_c^2)^2]/\sum[w(F_o^2)^2]\}^{1/2}$.

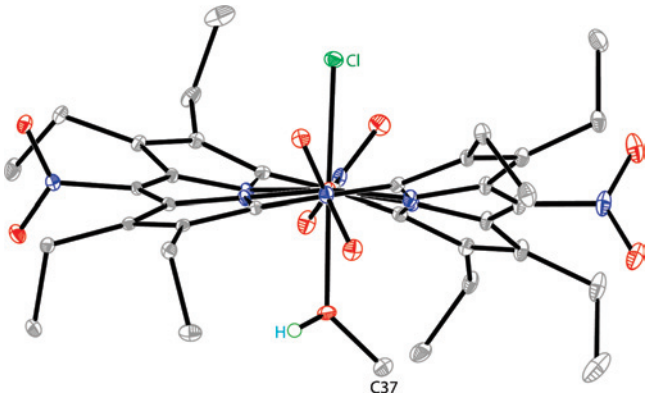

Figure 3. Perspective view of Fe^{III}(*tn*-OEP)(MeOH)Cl showing 50% thermal contours for all non-hydrogen atoms at 100 K (only methanolic hydrogen is shown for clarity).

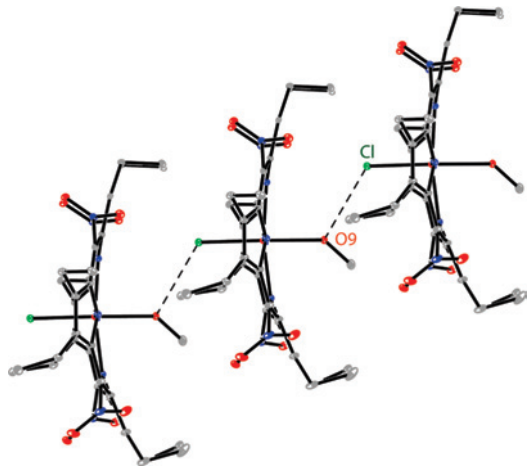

Figure 4. Hydrogen bonding interactions [O9···Cl, 3.031(4) Å] between the molecules in Fe^{III}(**tn**-OEP)(MeOH)Cl forming a linear extended chain (hydrogens are omitted for clarity).

porphyrin plane and 0.12 Å from the mean plane of the four porphinato nitrogens. Some measure of the asymmetry in axial ligand binding can be seen in the difference in axial bond lengths.

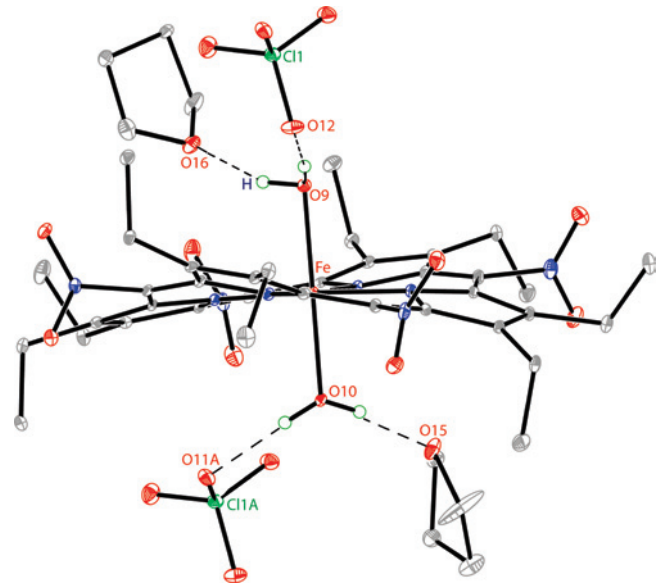

Figure 5. Perspective view of Fe^{III}(*tn*-OEP)$(H_2O)_2 \cdot ClO_4 \cdot$2THF showing 50% thermal contours for all non-hydrogen atoms at 100 K which also shows H-bonding interactions between the coordinated water and the solvent THF and ClO_4 (only hydrogens of coordinated water are shown for clarity). H-bonding distances (Å): O9···O16, 2.694(3); O9···O12, 2.734(3); O10···O15, 2.643(3); and O10···O11, 2.761(3).

Crystallographic Characterization of Fe^{III}(*tn*-OEP)$(H_2O)_2 \cdot ClO_4$. Dark brown colored crystals of Fe^{III}(*tn*-OEP)$(H_2O)_2^+$ were grown by slow diffusion of hexane into the THF solutions of the molecule at room temperature. The complex crystallizes in the triclinic space group $P\bar{1}$, and a perspective view is shown in Figure 5 which represents the first diaquo Fe(III) porphyrins in a distorted macocyclic environment while very few other reported[15] structures have almost planar porphyrin rings. An in-plane position of iron(III) atom in porphyrinato complexes has been demon-

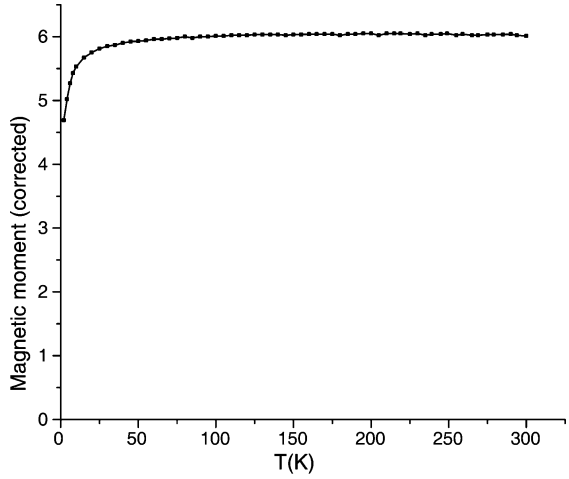

Figure 6. Magnetic moment of crystalline samples of Fe^{III}(*tn*-OEP)$(H_2O)_2 \cdot ClO_4$ as a function of temperature.

strated previously mostly for a low-spin six-coordinate derivative.[3−5] There is, however, one significant difference in the present structure and the structures of low-spin six-coordinate complexes. The average Fe−Np bond distance, which is 2.061(2) Å for Fe^{III}(*tn*-OEP)$(H_2O)_2^+$, is substantially longer than the 1.990 Å value typical for the low-spin derivatives. However, the average Fe−Np distance in Fe^{III}(*tn*-OEP)$(H_2O)_2^+$ is longest while the average Fe−O axial distance of 2.070(4) is the shortest compared to that for all other high-spin di aquo Fe(III)porphyrins reported so far.[15] Such an increase in the Fe−Np bond distance with the concomitant expansion of the porphyrinato core suggests significant population of the $3d_{x^2-y^2}$ orbitals.

Figure 5 also displays aspects of hydrogen bonding of the two aquo ligand (O9 and O10) protons with THF solvent molecules and to the perchlorate anion. One proton of an aquo ligand (O9) hydrogen bonds to the oxygen atom of the THF solvate molecule (with an O9···O16 distance of 2.694(3) Å) while the other proton forms a hydrogen bond to the O12 oxygen of the perchlorate counteranion (with an O9···O12 distance of 2.734(3) Å). Similar hydrogen bonding pattern also observed for the protons of other aquo ligand (O10) (O10···O15, 2.643(3) Å and O10···O11, 2.761(3) Å). Thus, Fe^{III}(*tn*-OEP)$(H_2O)_2^+$ ions are bridged by perchlorate anions via hydrogen bonds forming an infinite chain.

The variable temperature magnetic susceptibility of the polycrystalline samples of Fe^{III}(*tn*-OEP)$(H_2O)_2^+$ is substantially independent of temperature over the temperature range 5−300 K with an effective magnetic moment of 5.95 μ_B, which again confirms the high-spin nature of the complex; Figure 6 shows the plot of the effective magnetic moment as a function of temperature. A similar magnetic behavior is also observed for Fe^{III}(*tn*-OEP)Cl and Fe^{III}(*tn*-OEP)(MeOH)Cl with effective magnetic moments of 5.93 and 5.90 μ_B, respectively, at room temperature. The solution magnetic moments at 295 K in the purified dichloromethane, calculated by Evan's method,[16] are found to be 5.81, 5.91, and 5.88 MB for Fe^{III}(*tn*-OEP)Cl, Fe^{III}(*tn*-OEP)(MeOH)Cl, and Fe^{III}(*tn*-OEP)$(H_2O)_2^+$, respectively, which are again very close to the value obtained in the crystalline states.

^{1}H NMR spectra of the complexes (Supporting Information, Figure S1) obtained in $CDCl_3$ (after passing through basic alumina) at 295 K are in good agreement with a paramagnetic high-spin iron(III) porphyrin complex (S = 5/2). The signals are broad and the chemical shifts are temperature dependent. ^{1}H NMR studies have shown only one methylene resonance at 41.5 ppm for Fe^{III}(*tn*-OEP)Cl. One reason could be due to the fast ring inversion process in solution of the saddle distorted porphyrin macrocycle observed in the solid state, where the saddle porphyrinate ring inverts, such that the two pyrrole rings that were originally displaced above the mean plane of the macrocycle becomes displaced below and those that were originally displaced below become displaced above the mean porphyrin plane.[17] However, in five-coordinate Fe^{III}(*tn*-OEP)Cl, the $-CH_2$ protons should show two signals even if the ring inversion is fast in the NMR time scale. Another interpretation for the single resonance at 41.5 ppm could be the fast ligand (Cl^-) dissociation in the NMR time scale at 295 K. The similar ligand dissociations are seen earlier with ClO_4 in complexes such as Fe(OETPP)ClO_4, Fe(OMTPP)ClO_4, and Fe(TC_6TPP)ClO_4 where only one peak is observed for each phenyl-*ortho* and -*meta*, as well as CH_2 and CH_3 groups in OETPP and OMTPP and $CH_2(\beta)$ groups in TC_6TPP.[17c] However, the probability of such types of dissociations will be much less because of the substantial strong Fe−Cl bond although the exact reasons for single methylene resonance in Fe^{III}(*tn*-OEP)Cl are not clear at this moment. The methylene protons in Fe^{III}(*tn*-OEP)$(H_2O)_2^+$ also appears as a single peak at 52.6 ppm at 295 K, which become more and more broad as the temperature is lowered from 25 to −35 °C. When the temperature is lowered even further, this peak splits into two because the ring inversion process becomes so slow to be detectable by NMR spectroscopy. Axially coordinated water proton signals are also very broad and found at 11.2 ppm at 295 K (see Supporting Information, Figure S1). The Electron Paramagnetic Resonance (EPR) spectral measurements carried out at 77 K show similar features in solid and solution phase. Both spectra are axially symmetric with $g_\perp$ = 5.91 and $g_{||}$ = 2.01 for the frozen toluene solution and $g_\perp$ = 5.96 and $g_{||}$ = 2.03 for the powder (crushed single crystals, 77 K) for Fe^{III}(*tn*-OEP)(MeOH)Cl which are determined by the computer simulation of the observed spectra. Other two Fe(III) complexes also show

(14) (a) Einstein, F. W. B.; Willis, A. C. *Inorg. Chem.* **1978**, *17*, 3040. (b) Kirner, J. F.; Scheidt, W. R. *Inorg. Chem.* **1975**, *14*, 2081.
(15) (a) La, T.; Miskelly, G. M.; Bau, R. *Inorg. Chem.* **1997**, *36*, 5321. (b) Cheng, B.; Scheidt, W. R. *Acta Crystallogr.* **1995**, *C51*, 1271. (c) Korber, F. C. F.; Smith, J. R. L.; Prince, S.; Rizkallah, P.; Reynolds, C. D.; Shawcross, D. R. *J. Chem. Soc., Dalton Trans.* **1991**, 3291. (d) Scheidt, W. R.; Cohen, I. A.; Kastner, M. E. *Biochemistry* **1979**, *18*, 3546. (e) Kastner, M. E.; Scheidt, W. R.; Mashiko, T.; Reed, C. A. *J. Am. Chem. Soc.* **1978**, *100*, 666.
(16) Evans, D. F. *J. Chem. Soc.* **1959**, 2003.
(17) (a) Medforth, C. J. In *The Porphyrin Handbook*; Kadish, K. M., Smith, K. M., Guilard, R., Eds.; Academic Press: San Diego, 2000; Vol. *5*, Chapter 35, pp 70. (b) Yatsunyk, L. A.; Ogura, H.; Walker, F. A. *Inorg. Chem.* **2005**, *44*, 2867. (c) Yatsunyk, L. A.; Walker, F. A. *Inorg. Chem.* **2005**, *43*, 757. (d) Ogura, H.; Yatsunyk, L.; Medforth, C. J.; Smith, K. M.; Barkigia, K. M.; Renner, M. W.; Melamed, D.; Walker, F. A. *J. Am. Chem. Soc.* **2001**, *123*, 6564.

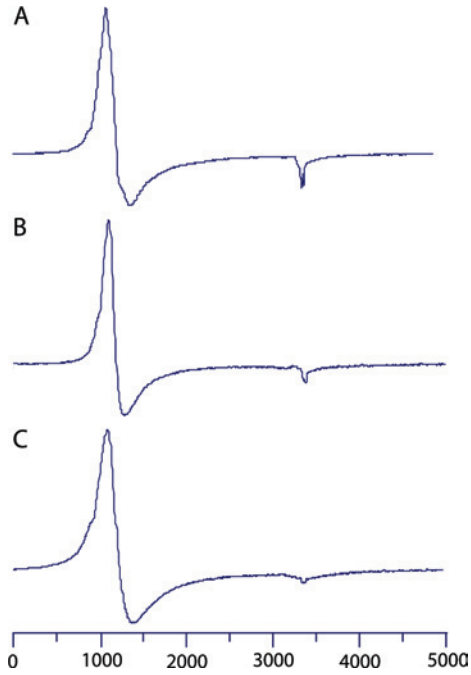

Figure 7. X-band EPR spectrum of (A) Fe^{III}(*tn*-OEP)Cl, (B) Fe^{III}(*tn*-OEP)(MeOH)Cl, and (C) Fe^{III}(*tn*-OEP)$(H_2O)_2 \cdot ClO_4$ in toluene at 77 K.

Table 3. Selected Geometrical Parameters

	Fe^{III}(*tn*-OEP)Cl	Fe^{III}(*tn*-OEP)(MeOH)Cl	Fe^{III}(*tn*-OEP)$(H_2O)_2 \cdot ClO_4$
Fe−Np[a]	2.067(3)	2.064(3)	2.061(2)
Fe−O/N(L)[a]		2.170(3)	2.070(4)
Fe−Cl (Å)	2.1918(10)	2.3049(11)	
$\Delta^{Fe}{}_{4N}$[b]	0.46	0.13	0.00
$\Delta^{Fe}{}_{24}$[c]	0.47	0.09	0.01
Φ_{pyr}[d]	19.33	19.3	14.3
Δ_{24}[e]	0.41	0.36	0.28
C_m[f]	0.06	0.05	0.17
C_β[f]	0.82	0.76	0.54
core size (Å)	2.014	2.060	2.061

[a] Average value in Å. [b] Displacement (in Å) of iron from mean plane of four pyrrole nitrogen. [c] Displacement (in Å) of iron from least-squares plane of porphyrin (24-atom). [d] Average angle (deg) between the mean porphyrin plane (24 atoms) and the pyrrole rings. [e] Average displacement (in Å) of the 24 atoms from the least-squares plane of the porphyrin. [f] Average displacement (in Å) from four porphyrinic nitrogen.

very similar features as shown in Figure 7. These results provide unequivocal evidence of high spin Fe(III) ($S = 5/2$) in both solid and solution phase.

Table 3 shows the comparison of the structures and geometrical features of all complexes reported here. It is interesting to note the stepwise out-of-plane displacements of iron: 0.47 Å for Fe^{III}(*tn*-OEP)Cl; 0.09 Å for Fe^{III}(*tn*-OEP)(MeOH)Cl, and 0.01 Å for Fe^{III}(*tn*-OEP)$(H_2O)_2^+$ from the porphyrin mean plane (24 atoms). In Fe^{III}(*tn*-OEP)-(MeOH)Cl, because of the coordination of weak MeOH, the Fe−Cl bond distance increases by ∼0.11 Å (as compared to the Fe−Cl distance in Fe^{III}(*tn*-OEP)Cl) while the Fe−O axial distance also lengthened by 0.10 Å as compared to the similar distances in Fe^{III}(*tn*-OEP)$(H_2O)_2^+$. However, the Fe−Np distances are quite comparable (within three sigma value) in all three Fe(III) complexes, but porphyrin cores have expanded significantly in the six-coordinated Fe(III) complexes reported here virtually to the same extent.

The porphyrin rings are highly distorted in all the

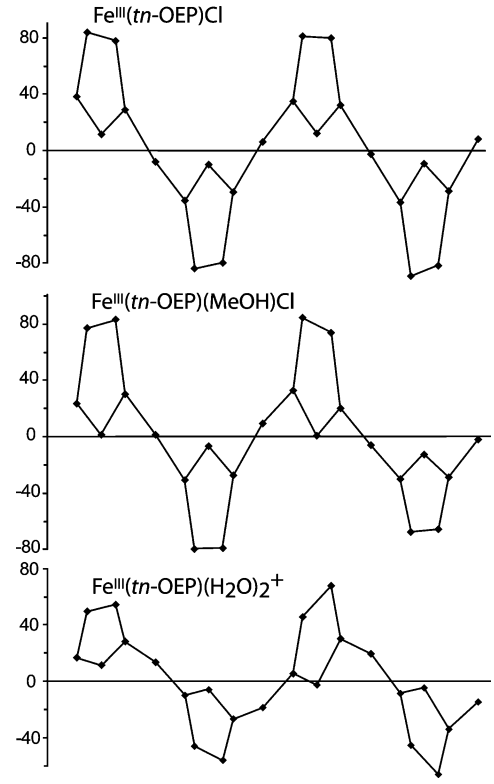

Figure 8. Out-of-plane displacements (in units of 0.01 Å) of the porphyrin core atoms from the mean porphyrin plane.

complexes and are best appreciated by turning to Figure 8 where the out-of-plane displacements, in units of 0.01 Å, of the core atoms are compared. The nomenclature that describes the types of distortions commonly observed in nonplanar porphyrins was originally suggested by Scheidt and Lee.[18] In a saddle conformation, alternate pyrrole rings tilt up and down with respect to the porphyrin mean plane (24 atoms) and the *meso* carbon atoms lie on the least-squares plane. In a ruffled conformation, alternate pyrrole rings twist clockwise or counterclockwise about the metal−nitrogen bond, and the *meso* carbon atoms move alternately above or below the least-squares plane of the 24 porphyrin atom core. As is evident from Figure 8, the ring distortions for all the three complexes can be described as of the purely saddle type with alternating displacement of the pyrrole rings below and above the mean porphyrin plane while the pyrrole nitrogen and *meso* carbons are placed on the plane. However, Shelnutt et al. has developed a normal-coordinate structural decomposition method (NSD)[19,20] which simulates any porphyrin distortion by linear combinations of six normal deformations that include, in addition to saddled (sad) and ruffled (ruf) distortions, domed (dom), waved (wav(x) and wav(y)), and propeller (pro) conformations, as well as yielding total out-of plane displacements (Doop).[19,20] The results of the NSD analysis of the complexes are presented

(18) Scheidt, W. R.; Lee, Y. J. *Struct. Bonding (Berlin)* **1987**, *64*, 1.
(19) (a) Jentzen, W.; Ma, J. -G.; Shelnutt, J. A. *Biophys. J.* **1998**, *74*, 753. (b) Jentzen, W.; Song, X.-Z.; Shelnutt, J. A. *J. Phys. Chem. B* **1997**, *101*, 1684.
(20) Sun, L.; Jentzen, W.; Shelnutt, J. A. *The Normal Coordinate Structural Decomposition Engine*; http://jasheln.unm.edu/jasheln/content/nsd/NSDengine.

Table 4. NSD of the Complexes

complex	*D*oop	B2u, saddle	B1u, ruffle	A2u, dome	Eg(*x*), wave(*x*)	Eg(*y*), wave(*y*)	A1u, propeller	sum	saddle/sum (%)	ruf/sum (%)
Fe^{III}(*tn*-OEP)Cl	2.5186	−2.5118	−0.1676	−0.0443	−0.0018	0.0622	−0.0175	2.8052	89.5	5.97
Fe^{III}(*tn*-OEP)(MeOH)Cl	2.3026	−2.2888	0.0750	0.1317	0.0186	−0.2000	−0.0091	2.7232	84.0	2.75
Fe^{III}(*tn*-OEP)$(H_2O)_2$. ClO_4	1.6926	1.6193	−0.4797	−0.0131	0.0343	0.1015	−0.0270	2.2749	71.2	21.08

Table 5. Six-coordinated High-Spin Fe(III) Complexes with Distorted Macrocycles

complex[a]	Fe−Np[c]	Fe−L_{ax}[c]	Δ_{24}[d]	$\Delta^{Fe}{}_{4N}$[e]	Ct···N	C_m[f]	C_β[f]	ref
Fe^{III}(TEP)$(THF)_2\cdot ClO_4$[b]	2.006(3)	2.160(2)	0.13	0.00	2.006	0.24	0.13	23a
Fe^{III}(TPP)$(EtOH)_2\cdot ClO_4$	2.034(2)	2.134(2)	0.07	0.00	2.033	0.03	0.24	23c
Fe^{III}(OEP)$(DMSO)_2\cdot PF_6$	2.035(9)	2.082(5)	0.15	0.00	2.035	0.28	0.12	23b
Fe^{III}(TPP)$(EtOH)_2\cdot BF_4$[b]	2.03(1)	2.142(9)	0.08	0.00	2.026	0.01	0.25	23d
Fe^{III}(TPP)$(EtOH)_2\cdot BF_4$	2.039(2)	2.116(2)	0.08	0.00	2.038	0.03	0.27	23c
Fe^{III}(TPP)$(OTeF_5)$(THF)	2.052(5)	1.967(5), 2.334(7)	0.06	0.19	2.043	0.11	0.25	13a
Fe^{III}(*tn*-OEP)(MeOH)Cl	2.064(3)	2.3049(11), 2.170(3)	0.36	0.13	2.060	0.05	0.76	this work
Fe^{III}(*tn*-OEP)$(H_2O)_2\cdot ClO_4$	2.061(2)	2.070(4)	0.28	0.00	2.061	0.17	0.54	this work

[a] Value in Å. [b] Admixed spin state between $S = 5/2$ and 3/2. [c] Average value. [d] Average displacement of the 24 atoms from the mean porphyrin plane. [e] Displacement of iron from mean plane of four pyrrole nitrogen. [f] Average displacement from four porphyrinic nitrogen.

in Table 4. The total distortions (*D*oop) decrease in the order Fe^{III}(*tn*-OEP)Cl > Fe^{III}(*tn*-OEP)(MeOH)Cl > Fe^{III}(*tn*-OEP)-$(H_2O)_2\cdot ClO_4$ while the core size increases (Table 3). Thus the porphyrin core is least distorted in Fe^{III}(*tn*-OEP)-$(H_2O)_2\cdot ClO_4$ while the core size is highest in the series. The large size of the high-spin iron(III) atom in Fe^{III}(*tn*-OEP)-$(H_2O)_2{}^+$ is accommodated by a substantial radial expansion of the porphyrin core with no displacement of the metal. Thus, a decrease in the out-of-plane displacement helps to bring the iron atom closer to porphyrin plane. Also, this expansion is accompanied by a significant decrease of the saddle distortion with a clear and significant increase in ruffling (Table 4). Moreover, X-ray crystallographic data[12] obtained for Fe^{II}(*tn*-OEP)$(L)_2$ shows that ferrous porphyrins are even more distorted than ferric, and saddling decreases sharply from ferric to ferrous while ruffling increases significantly.

However, there are several reports[21,22] of structurally characterized metalloporphyrins that have used *tn*-H_2OEP as porphyrin core. The addition of four electron withdrawing and bulky nitro groups in the *meso* positions causes significant distortion of the porphyrin macrocycle, and its strong electron-withdrawing character has significantly enhanced the relative affinity of the metal center for axial ligands. For example, in pyridine, both four- and six-coordinated forms are observed for Ni(OEP), whereas Ni(*tn*-OEP) yields only six-coordinated Ni(*tn*-OEP)$(py)_2$; the Ni−Np bond lengths (2.049(5) Å) are significantly elongated compared to those found in Ni(*tn*-OEP) (1.917(4) and 1.922(4) Å).[21a] However, in VO(*tn*-OEP)(L), (L: py, MeOH, THF), the average V−Np distances are significantly smaller than the similar distance found in five-coordinate vanadyl porphyrins.[22] In the case of Zn(*tn*-OEP), the addition of methanol produces a polymeric compound of the general formula $\{Zn^{II}(tn\text{-OEP})\}_n$ where polymer formation was achieved via the utilization of nitro oxygen atoms as axial ligands to the metal center of neighboring porphyrins.[21c] However, a series of five-coordinated Zn^{II}(*tn*-OEP)(L) (where, L: imi, 1-Meimi, 2-Meimi, etc.) was readily prepared by the addition of nitrogenous base as axial ligand (L) in which the Zn−Np distances (2.084(6) Å for L = imidazole; 2.086(3) Å for L = 1-Meimidazole, etc.) are significantly elongated compared to that of $\{Zn(tn\text{-OEP})\}_n$ (Zn−Np, 2.047(4)).[21b] The respective Co^{II}(*tn*-OEP) derivative also showed a polymeric structure $\{Co^{II}(tn\text{-OEP})\}_n$, isostructural to that described for $\{Zn^{II}(tn\text{-OEP})\}_n$.[21b] In the presence of pyridine as axial ligand, the monomeric six-coordinated Co^{II}(*tn*-OEP)$(py)_2$ was formed although no solid state structure is reported.[21b]

Table 5 shows structurally characterized[13a,23] six-coordinated high-spin Fe(III) complexes that have distorted porphyrin macrocycles; our complexes authenticate as having the most distorted macrocycle with significant increase of the average Fe−Np distance as well as the core size (a projection of the Fe−Np bond into the average plane of the macrocycle). In contrast, the Fe−Np distance and core size generally decreases with increasing nonplanarity of the porphyrin macrocycle.[1−5] Moreover, saddle shaped complexes are known to stabilize intermediate spin states with weak axial ligands.[3,5−8] For example, six-coordinate iron(III) complexes that contains highly saddle H_2OETPP forms Fe^{III}(OETPP)$(L)_2{}^+$ with weakly coordinated axial ligands (L: THF, 4-CNPy, Py, etc.) which have been interpreted to have very pure intermediate spin states.[5f−h] The major reasons for intermediate spin states were suggested to be (1) the short Fe−Np bond length commonly observed in highly deformed porphyrin complexes, (2) the weak coordinating ability of the axial ligands, and (3) the presence of saddle distorted porphyrin macrocycles.[5−8] However, the presence of four electron-withdrawing bulky nitro groups at the *meso* positions saddle-distort the porphyrin macrocycles significantly and

(21) (a) Barkigia, K. M.; Renner, M. W.; Senge, M. O.; Fajer, J. *J. Phys. Chem. B* **2004**, *108*, 2173. (b) Senge, M. O. *J. Porphyrins Phthalocyanines* **1998**, *2*, 107. (c) Senge, M. O.; Smith, K. M. *J. Chem. Soc., Chem. Commun.* **1994**, 623. (d) Senge, M. O. *J. Chem. Soc., Dalton Trans.* **1993**, 3539.

(22) Ghosh, S. K.; Patra, R.; Rath, S. P. *Inorg. Chem.* **2008**, *47*, 0000.

(23) (a) Ohgo, Y.; Soitoh, T.; Nakamura, M. *Acta Crystallogr.* **1999**, *C55*, 1284. (b) Mylrajan, M.; Anderson, L. A.; Sun, J.; Loehr, T. M.; Thomas, C. S.; Sullivan, E. P.; Thomson, M. A. J. R.; Long, K. M.; Anderson, O. P.; Strauss, S. H. *Inorg. Chem.* **1995**, *34*, 3953. (c) Scheidt, W. R.; Geiger, D. K.; Lee, Y. J.; Gans, P.; Marchon, J. C. *Inorg. Chem.* **1992**, *31*, 2660. (d) Gans, P.; Buisson, G.; Duee, E.; Regnard, J. R.; Marchon, J. C. *J. Chem. Soc., Chem. Commun.* **1979**, 393.

weaken the field strength of the pyrrole nitrogen that leads to significant increase in Fe−Np distances for the complexes reported here. Moreover, the electron withdrawing nitro substituents at the *meso* position reduce the electron density of the macrocycle particularly at the *meso* positions which should have a large impact on the energy levels of the porphyrin orbitals especially for a_{2u} because of its larger coefficients at the *meso* carbons, and, as a result, the interactions between porphyrin and metal orbitals are substantially less (vide infra) which probably is responsible for the "pure" high-spin nature for the complexes reported here.

For five-coordinated Fe^{III}(*tn*-OEP)Cl, it appears that the out-of-plane displacement (0.47 Å) of the iron atom depends on the optimization of the iron-ligand bonding within the coordination geometry. In the six-coordinated complex, the large high-spin iron(III) atom is known to be accommodated by a combination of core expansion and displacement of the iron (III) atom from the mean porphyrin planes.[3,10] However, in both five- and six-coordinated Fe(III) porphyrins reported here, the Fe−Np distances are quite comparable (within three sigma value), and the porphyrin cores have expanded significantly virtually to the same extent upon axial coordination forming Fe^{III}(*tn*-OEP)(MeOH)Cl and Fe^{III}(*tn*-OEP)$(H_2O)_2^+$. Thus, Fe atom in Fe^{III}(*tn*-OEP)(MeOH)Cl is not out of plane because of the larger atom size because the expanded cavity size could fit the atom nicely. When the axial ligands are equivalent as in Fe^{III}(*tn*-OEP)$(H_2O)_2^+$, the iron atom is constrained to lie in the heme plane with significant radial expansion and with lesser ring distortion. But when the ligands are not equivalent, as in Fe^{III}(*tn*-OEP)(MeOH)Cl, the displacement of the iron atom depends on the relative axial ligand bond strengths and also their nonbonded interactions with the pyrrole rings. The balance of these forces provides considerable flexibility in the axial geometry. However, the direction and amount of iron displacement depends on both the relative strength of the axial ligands and the nature and extent of porphyrin ring deformations.

Our demonstration suggests that the displacements of iron in proteins are the consequences of nonequivalent axial coordination, as well as the nature and extent of protein induced deformations at the heme. The different conformational landscapes observed further illustrate the plasticity of the macrocycles as well as their acute structural sensitivity to their microenvironment. The crystal structure of horse methemoglobin reveals small displacement of the iron atom from the heme plane (0.07 Å in the α chains and 0.21 Å in the β chains).[3,9] However, metHb and metMb have the same axial ligand set,[9,10] imidazole and water, and the porphyrin core size is expected to be very similar. Thus, it seems likely that the differences in the α and β subunits of the methemoglobins reflect protein constraints on heme stereochemistry.

In planar D_{4h} metalloporphyrins, the metal d orbitals and the porphyrin a_{1u} and a_{2u} highest occupied molecular orbitals (HOMOs) are orthogonal so no interactions can be expected between the a_{1u} or a_{2u} orbitals and iron d orbitals.[8] However, nonplanarity makes certain metal(d)−porphyrin(π) orbital interactions symmetry-allowed. For example, ruffling favors the metal (d_{xy})−porphyrin (a_{2u}) orbital interaction while saddling allows the metal ($d_{x^2-y^2}$)−porphyrin (a_{2u}) orbital interaction.[8] Thus, if the planar macrocycle is replaced by the saddled one, we can expect at least three bonding interactions between metal and porphyrin orbitals: (i) the less-effective nitrogen donation to the half-filled $d_{x^2-y^2}$ orbital, (ii) the interaction between the $d_{x^2-y^2}$ and a_{2u} orbitals, and (iii) the interaction between the d_{xy} and a_{1u} orbitals. However, the $d_{xy}-a_{1u}$ interaction is supposed to be quite small in the high-spin saddled complexes.[8b,c,i] Saddling inhibits the contact between the nitrogen lone pairs and metal $d_{x^2-y^2}$ orbital. Moreover, the presence of four electron withdrawing nitro substituents at the *meso* position reduces the electron density particularly at the *meso* positions, which should have large impact on the energy levels of the porphyrin orbitals especially for a_{2u} because of its larger coefficients at the *meso* carbons. Also, the Fe−Np distances are significantly large in the series and, as a result, the interaction between the iron $d_{x^2-y^2}$ and porphyrin a_{2u} orbital is less effective, so $d_{x^2-y^2}$ orbital is not destabilized as compared to d_{z^2} (which is the necessary condition for the intermediate spin state) and thus responsible for the high-spin nature of the Fe(III) complexes reported here.

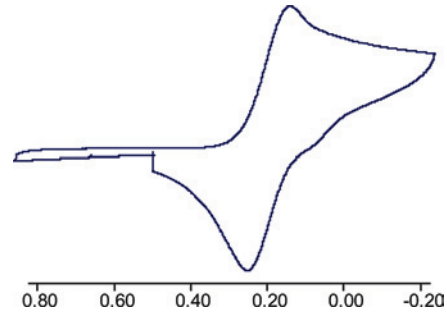

Figure 9. Cyclic voltammogram for Fe^{III}(*tn*-OEP)Cl in CH_2Cl_2 (scan rate 100 mV/s) with 0.1 M tetra(*n*-butyl)ammonium hexafluorophosphate as supporting electrolyte.

Cyclic Voltammetric Study. Cyclic voltammetric experiments on Fe^{III}(*tn*-OEP)Cl were done at 25 °C under N_2 in CH_2Cl_2 with 0.1 M tetrabutylammonium hexafluorophosphate (TBAH) as the supporting electrolyte, and the typical spectrum is shown in Figure 9. $E_{1/2}$ of the Fe^{III}/Fe^{II} reduction process of Fe^{III}(*tn*-OEP)Cl is observed at 0.20 V (ΔE_p, 70 mV), a considerably more positive value than those of Fe(OEP)Cl which were found at −0.49 V under identical conditions. However, the ring-centered oxidation of Fe^{III}(*tn*-OEP)Cl was not observed within the solvent limit (∼1.8 V) whereas oxidation of Fe^{III}(OEP)Cl was observed at 0.95 V. Moreover, the potentials did not alter the values with the nature of electrolyte counteranion (e.g., PF_6^-, ClO_4^-, Cl^-). It is thus easier to reduce Fe^{III}(*tn*-OEP)Cl than Fe^{III}(OEP)Cl by almost 700 mV, while oxidations are very difficult. Thus, the addition of four NO_2 groups in the porphyrin macrocycle serves both to protect the reactive *meso* position from rapid oxidative attack and to stabilize both porphyrin and metal against any oxidative degradation during catalysis; thus, Fe^{III}(*tn*-OEP)Cl ranks among the most effective catalysts in the oxygenation process.[24]

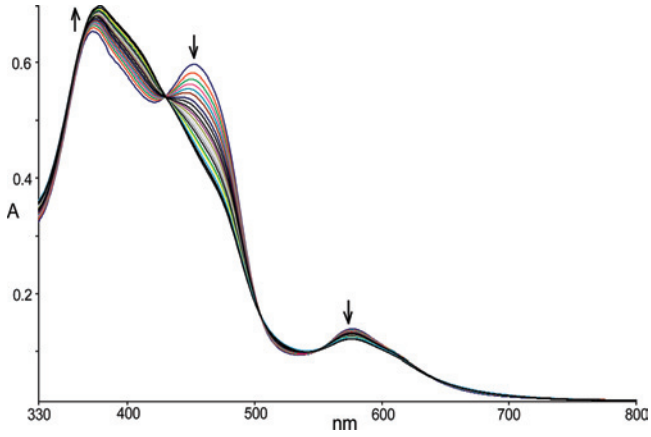

Figure 10. Autoxidation of $[Fe^{II}(tn\text{-OEP})Cl]^-$ in dichloromethane at 1 atm O_2 pressure at 295 K forming $Fe^{III}(tn\text{-OEP})Cl$, arrows indicate increase or decrease of band intensity. Isosbestic points (nm): 429, 503, 554, and 628.

Bulk reduction of dichloromethane solution of $Fe^{III}(tn\text{-OEP})Cl$ at a constant potential of 0.00 V in a nitrogen atmosphere changes the color from brown to green because of the formation of the iron(II) complex which shows a reversible oxidation at the same potential. Unlike most other iron(II) porphyrins, the electrochemically generated solutions of $[Fe^{II}(tn\text{-OEP})Cl]^-$ autoxidize very slowly (days) at 1 atm O_2 pressure. Figure 10 shows the autoxidation of $[Fe^{II}(tn\text{-OEP})Cl]^-$ at 295 K which reveals a clean isosbestic (429, 503, 554, and 628 nm) transformation between the iron(III) (378, 425 and 668 nm) and the iron(II) (373, 452, and 576) porphyrins. Moreover, the electronic absorption spectra for controlled-potential oxidation at 0.40 V of $[Fe^{II}(tn\text{-OEP})Cl]^-$ species, generated upon bulk reduction of $Fe^{III}(tn\text{-OEP})Cl$, exactly overlap with one another. Thus, it appears that the iron species remains five-coordinate with chloride in the axial position in the reduced species, and there is no loss of chloride ion in the process, otherwise the autoxidation could show nonisosbestic behavior.[24b−d]

However, addition of 3-Cl-pyridine to $Fe^{III}(tn\text{-OEP})Cl$ in air produces the diamagnetic air-stable $Fe^{II}(tn\text{-OEP})(3\text{-Cl-py})_2$. Cyclic voltammetry in CH_2Cl_2/0.1 M Bu_4NPF_6 showed that $Fe^{II}(tn\text{-OEP})(3\text{-Cl-py})_2$ is difficult to oxidize because of the multiple electron-withdrawing substituents, and $E_{1/2}$ for the reversible one-electron oxidation of Fe(II) to Fe(III) occurs at high positive potential (0.79 V) which readily explains why the complex in solution is so stable in air. Moreover, the $E_{1/2}$ value for the $Fe^{II/III}$ redox couple is remarkable in that it is shifted anodically ~600 mV relative to that observed for $[Fe^{II}(tn\text{-OEP})Cl]^-$, and metal centered redox processes are also found to be dependent on the basicity of axial ligands in $Fe^{II}(tn\text{-OEP})(L)_2$.[12] This large anodic shift illustrates the effective removal of metal-centered electron density by the macrocycle when the metal is constrained to reside in the porphyrin plane.

Conclusions

We have presented here a rare family of five- and six-coordinated high-spin Fe(III) porphyrins which demonstrates, for the first time, stepwise metal displacements in a single molecular framework that has generally been recognized in the biological systems. The introduction of four nitro groups into the *meso*-positions severely distorts the porphyrin geometry and provide an interesting modulation of the macrocycle properties which enables the facile isolation of high-spin $Fe^{III}(tn\text{-OEP})Cl$, $Fe^{III}(tn\text{-OEP})(MeOH)Cl$, and $Fe^{III}(tn\text{-OEP})(H_2O)_2^+$, for the first time, in a highly saddle distorted macrocyclic environment. In contrast, the saddle shaped complexes are known to stabilize the intermediate spin states with weak field axial ligands. The stepwise out-of-plane displacements of iron are as follows: 0.47 Å for $Fe^{III}(tn\text{-OEP})Cl$; 0.09 Å for $Fe^{III}(tn\text{-OEP})(MeOH)Cl$, and 0.01 Å for $Fe^{III}(tn\text{-OEP})(H_2O)_2^+$ from the mean plane of the porphyrins. The average displacements of porphyrin core atoms decreases in the order $Fe^{III}(tn\text{-OEP})Cl$ > $Fe^{III}(tn\text{-OEP})(MeOH)Cl$ > $Fe^{III}(tn\text{-OEP})(H_2O)_2\cdot ClO_4$ while the core size increases. Thus, the porphyrin core is least distorted in $Fe^{III}(tn\text{-OEP})(H_2O)_2\cdot ClO_4$ while the core size is highest in the series, and the large size of the high-spin iron(III) atom in $Fe^{III}(tn\text{-OEP})(H_2O)_2^+$ is now accommodated perfectly with no displacement of the metal. Thus, a decrease in the out-of-plane displacement helps to bring the iron atom closer to the porphyrin plane. Also, the core expansion is accompanied by a significant decrease of the saddle distortion with a clear and significant increase in ruffling. Our characterization demonstrates that increase in ruffling and/or decrease in macrocycle deformation brings the iron atom more into the plane in a distorted macrocyclic environment.

However, in both five- and six-coordinated Fe(III) porphyrins, the Fe−Np distances are quite comparable and the porphyrin cores have expanded significantly from five to six coordination virtually to the same extent in $Fe^{III}(tn\text{-OEP})(MeOH)Cl$ and $Fe^{III}(tn\text{-OEP})(H_2O)_2^+$. Thus Fe atom in $Fe^{III}(tn\text{-OEP})(MeOH)Cl$ is not out of plane because of the larger atom size since the expanded cavity size could fit the atom nicely. Presumably, the displacement of the iron atom is dependent on the relative importance of the bonding of the two dissimilar axial ligands, as well as the ring deformation. Some measure of the asymmetry in axial ligand binding can be seen in the difference in the axial bond lengths. Thus, our demonstrations suggest that the displacements of iron in proteins are the consequences of nonequivalent axial coordination, as well as protein induced deformation at the heme. However, metHb and metMb have the same axial ligand set, imidazole and water, and the porphyrin core size is expected to be very similar in both cases. Thus, it seems likely that the differences in the α and β subunits of the methemoglobins reflect protein constraints on heme stereochemistry. The high-spin nature of the complexes reported here is believed to be due to the larger Fe−Np distances

(24) (a) Grinstaff, M. W.; Hill, M. G.; Labinger, J. A.; Gray, H. B. *Science* **1994**, *264*, 1311. (b) Moore, K. T.; Fletcher, J. T.; Therien, M J. *J. Am. Chem. Soc.* **1999**, *121*, 5196. (c) Grinstaff, M. W.; Hill, M. G.; Birnbaum, E. R.; Schaefer, W. P.; Labinger, J. A.; Gray, H. B. *Inorg. Chem.* **1995**, *34*, 4896. (d) Wijesekera, T.; Matsumoto, A.; Dolphin, D.; Lexa, D. *Angew. Chem.* **1990**, *29*, 1028. (e) Chang, C. K.; Barkigia, K. M.; Hanson, L. K.; Fajer, J. *J. Am. Chem. Soc.* **1986**, *108*, 1352. (f) Barkigia, K. M.; Palacio, M.; Sun, Y.; Nogues, M.; Renner, M. W.; Varret, F.; Battioni, P.; Mansuy, D.; Fajer, J. *Inorg. Chem.* **2002**, *41*, 5647.

and also the presence of strong electron withdrawing nitro groups at the *meso* positions which reduce substantially the interaction between the iron $d_{x^2-y^2}$ and the porphyrin a_{2u} orbital.

Electrochemical data obtained from the cyclic voltammetric study reveals that the metal reduction potential of Fe^{III}(*tn*-OEP)Cl is observed at 0.20 V (ΔE_p, 70 mV) which shows a ~700 mV more anodic shift compared to those of Fe(OEP)Cl. However, the ring-centered oxidation of Fe^{III}(*tn*-OEP)Cl was not observed within the solvent limit (~1.80 V). Thus, the addition of four NO_2 groups in the porphyrin macrocycle serves both to protect the reactive *meso* position from rapid oxidative attack and to stabilize both porphyrin and metal against any oxidative degradation during any catalytic oxygenation process. Moreover, the addition of 3-Cl-pyridine to Fe^{III}(*tn*-OEP)Cl in air produces a very rare air-stable Fe^{II}(*tn*-OEP)(3-Cl-py)$_2$; $E_{1/2}$ for the $Fe^{II/III}$ oxidation occurs at high positive potential of 0.79 V which is ~600 mV more anodic than $[Fe^{II}$(*tn*-OEP)Cl$]^-$. This large anodic shift illustrates the effective removal of metal-centered electron density by the macrocycle when the metal is constrained to reside in the porphyrin plane.

Experimental Section

Materials. Reagents and solvents were purchased from commercial sources and purified by standard procedures before use. Grade-I neutral alumina was used for column chromatography. H_2OEP[25] and tetranitrooctaethylporphyrin (*tn*-H_2OEP)[11] were prepared by literature methods.

Preparation of Fe^{III}(*tn*-OEP)Cl. Iron was inserted in *tn*-H_2OEP by a standard procedure[26] under a dioxygen-free dinitrogen atmosphere to produce Fe^{III}(*tn*-OEP)Cl. The solid product was redissolved in dichloromethane and washed with an aqueous 0.2 M hydrochloric acid solution. The dichloromethane solution was then dried with sodium sulfate and evaporated to dryness. The product was purified by column chromatography on silica gel with chloroform as an eluent. The red band was collected and evaporated to dryness to obtain a brown solid. Yields: 90 mg (80%). Anal. Calcd (found): C, 57.83 (57.88); H, 5.02 (5.10); N, 13.95 (13.90). UV−vis (chloroform) [λ_{max}, nm (ε, M^{-1} cm^{-1})]: 378 (2.5×10^4), 425 (1.76×10^4), and 668 (1.2×10^3). μ_{eff} (295 K, crystalline solid), 5.93 μ_B EPR data: in solid (77K), $g_\perp = 5.98$ and $g_\parallel = 2.01$; in toluene (77K), $g_\perp = 5.96$ and $g_\parallel = 2.01$. ^{1}H NMR ($CDCl_3$, 295 K): CH_2: 41.5; −CH_3: 5.25 ppm.

Preparation of Fe^{III}(*tn*-OEP)(MeOH)Cl. Fe^{III}(*tn*-OEP)Cl (25 mg, 0.03 mmol) was dissolved in 3 mL of chloroform and stirred for 5 min. The solution was filtered to remove any solid residue and then carefully layered with dry methanol. On standing for 7−8 days, a dark purple crystalline solid was formed which was collected by filtration and dried in vacuum. Yields: 20 mg (75%). Anal. Calcd (found): C, 53.20 (53.15); H, 5.31 (5.38); N, 13.41 (13.48). UV−vis (chloroform) [λ_{max}, nm (ε, M^{-1} cm^{-1})]: 381 (2.4×10^4), 431 (1.7×10^4), and 670 (1.3×10^3); μ_{eff} (295 K, crystalline solid), 5.90 μ_B EPR data: in solid (77 K), $g_\perp = 5.96$ and $g_\parallel = 2.03$; in toluene (77 K), $g_\perp = 5.93$ and $g_\parallel = 2.01$.

Preparation of Fe^{III}(*tn*-OEP)$(H_2O)_2\cdot ClO_4$. Fe^{III}(*tn*-OEP)Cl (100 mg, 0.12 mmol) was dissolved in 100 mL of dichloromethane and 100 mL of 2 M aqueous sodium hydroxide was added to it and stirred for 1 h. The organic layer was separated and washed with water till free from NaOH which was then dried over anhydrous Na_2SO_4. The resulting solution was then evaporated to dryness and purified by column chromatography using basic alumina. The major green fraction eluted with dichloromethane was collected and vaccuum-dried to obtained a dark brown solid. The solid thus obtained was dissolved in 100 mL of dichloromethane, $Fe(ClO_4)_3\cdot 9H_2O$ (200 mg) was added to it and stirred for 2 h, which was then filtered off to remove inorganic solids and evaporated to dryness. The solid was redissolved in THF and then carefully layered with cyclohexane. On standing for 6−7 days, a dark crystalline solid was formed which was isolated by filtration, washed with cyclohexane, and dried in vacuum. **Caution!** *Perchlorate salts are potentially explosive when heated or shocked. Handle them in milligram quantities with care.* (Yield 78.5 mg, 70%). Anal. Calcd (found): C, 47.80 (47.74); H, 4.91 (5.00); N, 12.40 (12.45). UV−vis (chloroform) [λ_{max}, nm (ε, M^{-1} cm^{-1})]: 392 (2.7×10^4); μ_{eff} (295 K, crystalline solid), 5.95 μ_B EPR data: in solid (77 K), $g_\perp = 5.96$ and $g_\parallel = 2.03$; in toluene (77 K), $g_\perp = 5.91$ and $g_\parallel = 2.01$. ^{1}H NMR ($CDCl_3$, 295 K): CH_2: 52.6; −CH_3: 6.72; −OH_2: 11.2 ppm.

Preparation of Fe^{II}(*tn*-OEP)(3-Cl-py)$_2$. Fe^{III}(*tn*-OEP)Cl (25 mg, 0.03 mmol) was dissolved in 10 mL of dichloromethane and 0.5 mL of 3-Chloro pyridine was added to it and was stirred for 2 h; the initial brown solution turned green during the progress of the reaction. The resulting solution thus obtained was evaporated to dryness to obtained a dark green solid. The solid was redissolved in chloroform containing 3% 3-chloro pyridine and then carefully layered with cyclohexane. On standing for 6−7 days, a dark crystalline solid was formed which was then isolated by filtration, washed with cyclohexane and dried in vacuum. (Yield 27 mg, 90%) Anal. Calcd (found): C, 55.50 (55.47); H, 4.82 (4.89); N, 14.08 (14.14). UV−vis (chloroform) [λ_{max}, nm (ε, M^{-1} cm^{-1})]: 381 (2.85×10^4), 426 (2.8×10^4), 548 (5.2×10^3), and 584 (5.1×10^3). ^{1}H NMR ($CDCl_3$, 295 K): CH_2: 3.01; −CH_3: 1.17 ppm.

Instrumentation. UV−vis spectra were recorded on a PerkinElmer UV/vis spectrometer. Elemental (C, H, and N) analyses were performed on a Perkin-Elmer 2400II elemental analyzer. EPR spectra were obtained on a Bruker EMX EPR spectrometer. Cyclic voltammetric studies were performed on a BAS Epsilon electrochemical workstation in dichloromethane with 0.1 M tetra-*n*-butylammonium hexafluorophosphate (TBAH) or tetra-*n*-butylammonium ammonium perchlorate (TBAP) as supporting electrolyte. The working electrode was a BAS glassy carbon disk electrode of radius 3 mm, the reference electrode was Ag/AgCl, and the auxiliary electrode was a Pt wire. The concentration of the compounds was in the order of 10^{-3} M. The ferrocene/ferrocenium couple occurs at $E_{1/2} = +0.45$ (65) V versus Ag/AgCl under the same experimental conditions. Magnetic susceptibility data were collected using a Quantum Design MPMS SQUID magnetometer over the temperature range 5−300 K. Data were collected in applied fields of 1 T and corrected for diamagnetism using Pascal's constants.[1] H NMR spectra were recorded on a JEOL 500 MHz instrument. The spectra were recorded over a 100 kHz bandwidth with 64 K data points and a 5 ms 90° pulse. For a typical spectrum between 2000 and 3000 transients were accumulated with a 50 μs delay time. The residual ^{1}H resonances of the solvents were used as a secondary reference.

Structure Solution and Refinement. Crystals were coated with light hydrocarbon oil and mounted in the 100 K dinitrogen stream of a Bruker SMART APEX CCD diffractometer equipped with CRYO Industries low-temperature apparatus, and intensity data were collected using graphite-monochromated Mo Kα radiation (λ

(25) Sessler, L. J.; Mozaffari, A.; Johnson, M. R. *Org. Synth.* **1992**, *70*, 68.
(26) Adler, A. D.; Lango, F. R.; Kampas, F. *J. Inorg. Nucl. Chem.* **1970**, *32*, 2443.

= 0.71073 Å). The data integration and reduction were processed with the SAINT[27] software. An absorption correction was applied.[28] Structures were solved by the direct method using SHELXS-97 and refined on F^2 by a full-matrix least-squares technique using the SHELXL-97[29] program package. Non-hydrogen atoms were refined anisotropically. In the refinement, hydrogens were treated as riding atoms using the SHELXL default parameters. Crystal data are given in Table 2.

(27) *SAINT+*, 6.02 ed.; Bruker AXS, Madison, WI, 1999.
(28) Sheldrick, G. M. *SADABS 2.0*; University of Göttingen: Göttingen, Germany, 2000.
(29) Sheldrick, G. M. *SHELXL-97: Program for Crystal Structure Refinement*; University of Göttingen: Göttingen, Germany, 1997.

Acknowledgment. We are thankful to the Department of Science and Technology, Government of India, for financial support, including support for a CCD X-ray diffractometer and EPR facility at IIT Kanpur. R.P., A.C., and S.K.G. thank CSIR, India for fellowship. The authors thank Prof. Marilyn M. Olmstead for some valuable advice in a crystallographic problem.

Supporting Information Available: ^{1}H NMR spectra (Figure S1) and X-ray crystallographic details in CIF format. This material is available free of charge via the Internet at http://pubs.acs.org.

IC800944Q